Coarsening of foams driven by concentration gradients of gases of different solubilities

Benjamin Dollet

Coarsening of foams driven by concentration gradients of gases of different solubilities

Benjamin Dollet*

Univ. Grenoble Alpes, CNRS, LIPhy, 38000 Grenoble, France

E-mail: benjamin.dollet@univ-grenoble-alpes.fr

Abstract

The evolution of a foam driven by the transfer of two gases of different solubilities across the soap films is studied. A bamboo foam, or a train of films, is used as a model system; it is made of a poorly soluble gas, and put into contact with a reservoir of a soluble gas at an initial time. The measurement of the time evolution of the volume of each bubble shows that the foam swells, as it progressively incorporates the soluble gas. The dynamics is modelled from the gas fluxes across each film. The continuous limit of this model at large number of bubbles is studied in details: it gives an effective nonlinear diffusion equation, which fits the data very well. The corresponding diffusion constant, given by the product of the permeability of the soluble gas and the initial size of the bubbles, is shown to be the key parameter governing the coarsening dynamics of the foam.

Keywords

foams, permeability, gas mixtures, effective diffusion, films, interfacial barrier

Introduction

Liquid foams are intrinsically metastable systems, and evolve by three mechanisms:[1] drainage, coarsening, and coalescence, which are often coupled. Coarsening is the evolution process characterised by gas exchange between bubbles of different pressures, a process known as Ostwald ripening. When the foam contains a single gas, the gas flux between two bubbles separated by a soap film is proportional to their pressure difference, the area of the film, the solubility of the gas (usually quantified by Henry's constant[2]) and inversely proportional to the film thickness. Small bubbles tend to be convex and large bubbles concave, hence small bubbles tend to have a Laplace overpressure with respect to the bigger ones. Hence, overall, the bigger bubbles grow at the expense of smaller ones, which eventually disappear. This leads to the classical picture of coarsening, characterised by a increase of the mean bubble size with time.

In applications, such a drift of the bubble size is often detrimental. In order to minimise coarsening or even arrest it, a lot of research have focussed on the role of surfactants as interfacial barriers to gas transfer,[3–6] or on the blocking effect of particles adsorbed at the interfaces.[7,8] Another simple solution consists in using relatively insoluble gases,[9,10] like perfluorohexane (C_6F_{14}) or perfluoroethane (C_2F_6). Indeed, a drastic decrease of the coarsening rate has been evidenced in a foam made of C_2F_6 compared to a foam made of N_2, which is much more soluble.[11] Not only do insoluble gases slow down coarsening, but they also slow down drainage[12] and coalescence.[13]

However, this description of coarsening is valid only inside the foam bulk. A different coarsening process arises at the boundary between air and a foam made with a different gas. In particular, when the gas in the foam is less soluble than air, it has been shown that the foam spontaneously swells from its boundary by incorporating air.[14] This has been ascribed to a new driving force, distinct from the difference of Laplace pressure previously described: it is now the difference of partial pressures across soap films which dominates gas transfer. Hence, air tends to enter the foam, while the less soluble gas inside tends to leak away.

However, because of the solubility contrast, the transfer rate of air is higher than that of the less soluble gas: hence, there is a net flux towards the foam, which explains its swelling.

Another consequence of this process is that the gas content inside such a foam continuously evolves, as more and more air is incorporated. While generally overlooked, this evolution of the gas content is relevant in foam acoustics, where the speed of sound is close to that of the gas at large enough frequency or bubble size.[15,16] In particular, Pierre et al.[17] have observed that, starting from a C_2F_6 foam placed in air, the acoustic response at long times is compatible with a foam made of air. However, the dynamics of this evolution has not been quantified; experimentally, it is challenging, owing to the difficulty to measure in situ gas contents. Most experimental studies on the exchange of different gases through liquid films have focussed on single bubbles[18–21] or single films.[22–24] Although useful, such measurements do not capture the full dynamics of gas exchanges through foams, which has hitherto been considered by only a few studies.[25–27]

In this paper, we study in detail, experimentally and theoretically, the coarsening dynamics of a model foam made of an insoluble gas and in contact with air. As a model foam, we use the so-called bamboo foam, i.e. a train of soap films inside a tube. While retaining the essential ingredient of having layers (here, single bubbles) of different "depths" counted from the interface between the foam and the outer atmosphere, this system has two major advantages. (i) Its evolution is easy to track by imaging the film displacements; and (ii) the films are flat, ensuring that the evolution is driven solely by gradients of composition, and not by differences of Laplace pressure.

The paper is organised as follows. We first present our experimental methods and results in Sec. . The theoretical model is introduced in Sec. . An effective diffusion approach derived from this model, and its comparison with the experimental data, is presented in Sec. . The deduced value of the permeability of the soluble gas is discussed in Sec. , and compared with other values from the literature. Conclusions are drawn in Sec. .

Experiments

Materials and methods

We study the coarsening dynamics of a foam prepared with pure C_2F_6 as a gas, and put in contact with pure nitrogen. In order to simplify the geometry and to be able to visualise coarsening in each bubble, we use a bamboo foam, consisting of a train of consecutive soap films in a glass tube of length 60 cm and radius $a = 4.4$ mm. We use as a surfactant solution a mixture of sodium lauryl-dioxyethylene sulfate (SLES), cocoamidopropyl betaine (CAPB) and myristic acid (MAc), prepared as described in.[28]

Prior to the experiment, the glass tube is positioned at a small tilt angle (about 10 degrees from the horizontal), and is open at both ends. We inject some solution with a syringe at the top end. After less than one minute, some solution accumulates at the bottom open end, the excess of solution being let to drip freely; enough solution remains in the tube to form a small reservoir filling the bottom end. Perfluoroethane (C_2F_6) supplied from a compressed gas bottle (Air Liquide) is injected through a flexible tube, with a controlled flow rate of 10 mL/min. This value was chosen after scanning different flow rates, because it gave the most monodisperse bubbles. This tube is first flushed with C_2F_6 long enough that we can safely consider that traces of air are in negligible amount. It is then manually plugged at the bottom end of the glass tube. The gas bubbling in the soap reservoir creates bubbles which arrange as a bamboo foam in the tube (Fig. 1a) containing at least 30 bubbles. The foam is generated in about 1 min. As bubbles are created, they entrain some liquid and the reservoir is progressively exhausted, leading to a slow progressive increase of the bubble length. Bubbling is stopped when the new bubbles become too much larger than the first ones.

Another flexible plastic tube is then manually introduced within the glass tube from its top end. Nitrogen is injected through this plastic tube, at a controlled rate of 30 mL/min. This tube has two functions: first, it is used to burst the first soap films by direct contact,

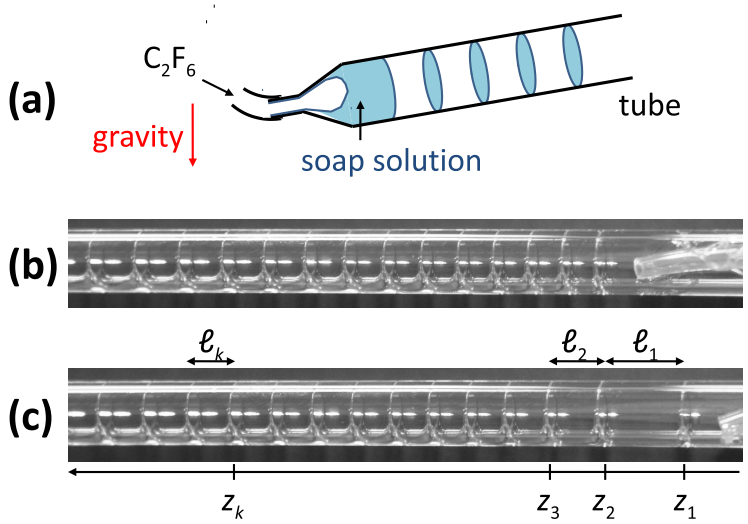

Figure 1: (a) Sketch of the bubbling process creating the films: C_2F_6 is injected at the bottom of a tilted tube through a reservoir of soap solution, generating a train of films in the tube. Snapshots of a train of films (b) at the beginning and (c) at the end of one experiment (corresponding to the data of Fig. 2c). The positions z_k of the films and the bubble lengths ℓ_k are overlaid for clarity.

and second, it continuously flushes the space in front of the first soap film with nitrogen. Nitrogen is supplied by a compressed gas bottle (Air Liquide) and let to flow through water, in order to saturate it with water vapour, to avoid vaporisation and early bursting of the soap films. This procedure ensures both that the initial condition is the closest possible to a bamboo foam of pure C_2F_6, and that the foam is in contact with pure nitrogen. Specifically, the flushing flow rate of 30 mL/min was chosen because it ensured that traces of C_2F_6 crossing the first film were flushed almost instantaneously, so that we could safely neglect the concentration of C_2F_6 outside the foam.

The foam is imaged with a high-resolution camera, and photographs are automatically recorded every 3 s in time-lapse mode. The beginning of the experiment is taken as the first image after the bursting of the first few films (because their mutual distance are often irreproducible) by direct contact with the plastic tube. It ends when a film first spontaneously bursts during coarsening. Meanwhile, the bubbles swell and expand downstream the tube: the position of the flexible tube flushing nitrogen is manually adjusted such that it remains

between 3 and 10 mm from the first soap film.

To analyse the recorded images, a spatiotemporal diagram is extracted using the freeware ImageJ, along a line drawn along the symmetry axis of the bamboo foam. On such a diagram, each soap film k ($1 \leq k \leq N_{\text{films}}$, with N_{films} the number of films) is identified as a bright line. The position $z_k(t)$ of this line is automatically extracted using a home-made Matlab routine, and the length $\ell_i(t)$ of each bubble is computed as: $\ell_i = z_i - z_{i+1}$ ($1 \leq i \leq N = N_{\text{films}} - 1$, with N the number of bubbles), see Fig. 1c. Our measurements thus consist of the evolution of the length of each bubble during the experiment.

Results

We performed three different experiments, with different initial bubble lengths, but with an initial preparation as monodisperse as possible (see insets of Fig. 2). The time evolution of some bubble lengths is shown in Fig. 2 until a film pops. All bubble lengths increase in time, and the rate of increase is larger for the bubbles closest to the outer environment (Fig. 1b and c). This qualitative observation is in agreement with the fact that the bubbles initially contain a more insoluble gas than the outside environment, which thus "feed" them progressively over time, starting from the first bubble in contact with the outer atmosphere, and then deeper inside the bubble assembly. The deepest bubble reported in Fig. 2, $i = 13$ in Fig. 2a, displays almost no evolution during the experiment. We can also observe some difference in trends, especially for the first bubble: while the time evolution of its length shows a clear concavity for the smallest initial length (Fig. 2a), its increase is almost linear, albeit with some irregular inflections, in the two other cases (Fig. 2b and c).

Theory

In this Section, we model the coarsening of a foam consisting of a mixture of two gases. The building block of the coarsening theory is the flux of gas through a liquid film of cross-section

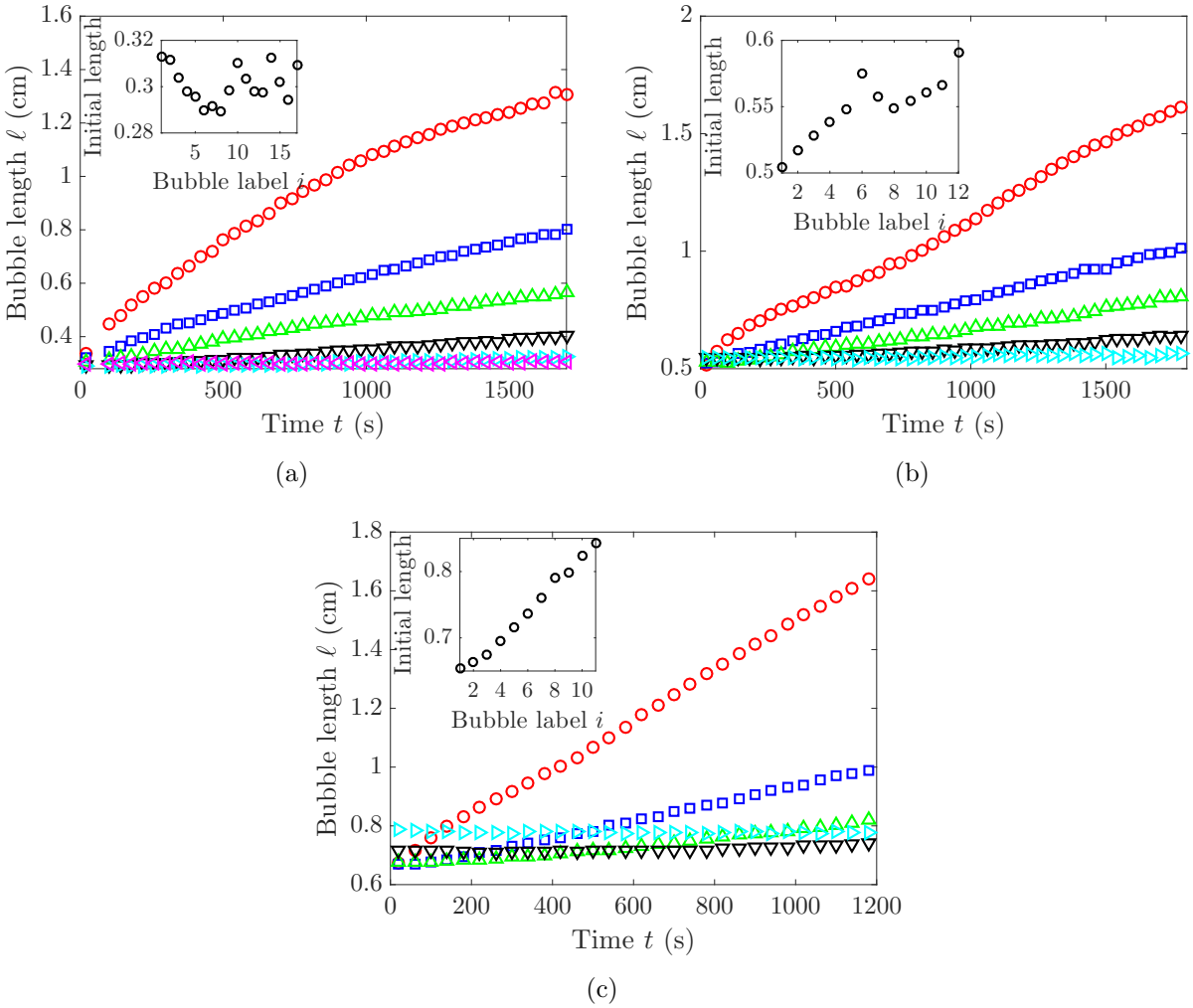

Figure 2: Time evolution of the length of a selection of bubbles within a train of films initially filled with C_2F_6 and put into contact with N_2: $i = 1$ ($\circ$), 2 ($\square$), 3 ($\triangle$), 5 ($\triangledown$), 8 ($\triangleright$) and 13 ($\triangleleft$, panel a only), counted from the N_2 reservoir inwards. The three panels correspond to different initial bubble lengths ℓ_0: (a) $\ell_0 = (0.30 \pm 0.01)$ cm, (b) $\ell_0 = (0.55 \pm 0.02)$ cm and (c) $\ell_0 = (0.74 \pm 0.07)$ cm. Insets: initial bubble length (in cm) as a function of i.

S. Princen and Mason[18] showed that if there is a molar concentration difference ΔC across the film, the molar gas flux towards the low concentration side equals $j = -kS\Delta C$, with k the gas permeability, a quantity having the dimensions of a velocity. Using the pressure difference $\Delta P = RT\Delta C$ holding for ideal gases, with $R = 8.314\ \mathrm{J \cdot mol^{-1} \cdot K^{-1}}$ the ideal gas constant and T the temperature, one gets:

$$j = \frac{kS}{RT}\Delta P. \tag{1}$$

Since the films are flat, there is no Laplace pressure, and the pressure in each bubble equals the ambient pressure P_{atm}. It equals the sum of the partial pressure of each of the two gases, denoted with superscripts 1 and 2 : $P_{\mathrm{atm}} = p^1 + p^2$. Let x the molar fraction of gas 2, then $p^2 = xP_{\mathrm{atm}}$ and $p^1 = (1-x)P_{\mathrm{atm}}$. If a given film separates two bubbles with a molar fraction difference Δx, the partial pressure difference equals $\Delta x P_{\mathrm{atm}}$ for gas 2, and is opposite for gas 1. Hence, after (1), the flux of gas 1 across the film is:

$$j^1_{x\to x+\Delta x} = \frac{k_1 S}{v_m}\Delta x, \tag{2}$$

and similarly for gas 2:

$$j^2_{x\to x+\Delta x} = -\frac{k_2 S}{v_m}\Delta x, \tag{3}$$

where k_i is the permeability of gas i, and $v_m = RT/P_{\mathrm{atm}} = 2.40 \times 10^{-2}\ \mathrm{m^3 \cdot mol^{-1}}$ the molar volume, which value is given at the experimental conditions $T = 293$ K and $P_{\mathrm{atm}} = 1.02 \times 10^5$ Pa. We shall henceforth take the convention that $k_1 > k_2$; hence, in the present case, gas 1 is N_2 whilst gas 2 is C_2F_6.

In what follows, we present a simple one-dimensional model based on these fluxes, which is adapted to bamboo foams in a tube of section S. We assume that within each bubble, gas interdiffusion is fast enough that the molar fraction is uniform. We thus consider an assembly of N bubbles, separated by films of section S and thickness h. The bubble i, where

$1 \leq i \leq N$, has a volume $V_i(t) = S\ell_i(t)$ with $\ell_i(t)$ its length along the tube, a number of moles $n_i^j(t)$ of gas j, where $j = 1$ or 2, and a molar fraction $x_i(t)$ of gas 2. The variation of n_i^j is determined by the flux of gas j from neighbouring bubbles $i-1$ and $i+1$. After (2), we can write:

$$\frac{\mathrm{d}n_i^1}{\mathrm{d}t} = j_{i-1\to i}^1 + j_{i+1\to i}^1 = \frac{k_1 S}{v_m}(-x_{i-1} + 2x_i - x_{i+1}), \tag{4}$$

and similarly, from (2):

$$\frac{\mathrm{d}n_i^2}{\mathrm{d}t} = j_{i-1\to i}^2 + j_{i+1\to i}^2 = -\frac{k_2 S}{v_m}(-x_{i-1} + 2x_i - x_{i+1}). \tag{5}$$

Since by definition $x_i = n_i^2/(n_i^1 + n_i^2)$, Eqs. (4) and (5) constitutes a system of $2N$ coupled nonlinear ODEs which determines the evolution of the system. It can be solved if the initial gas composition, given by $n_i^j(t = 0)$, is known. Finally, if bubble N is in contact with a wall with no flux of gas, Eqs. (4) and (5) are replaced by $\mathrm{d}n_N^1/\mathrm{d}t = j_{N-1\to N}^1 = k_1 S(-x_{N-1} + x_N)/v_m$ and $\mathrm{d}n_N^2/\mathrm{d}t = j_{N-1\to N}^2 = -k_2 S(-x_{N-1} + x_N)/v_m$.

Instead of writing the evolution in terms of the number of moles, we can write it in terms of the molar fraction and length of the bubbles ℓ_i. Since $x_i = n_i^2/(n_i^1 + n_i^2)$ and $\ell_i = (n_i^1 + n_i^2)v_m/S$, with v_m the molar volume of the gases, we get after some algebra:

$$\frac{\mathrm{d}\ell_i}{\mathrm{d}t} = (k_1 - k_2)(-x_{i-1} + 2x_i - x_{i+1}), \tag{6}$$

and:

$$\frac{\mathrm{d}x_i}{\mathrm{d}t} = -\frac{1}{\ell_i}[x_i k_1 + (1 - x_i)k_2](-x_{i-1} + 2x_i - x_{i+1}). \tag{7}$$

The permeabilities need not be constant in the current modelling. In what follows, we will consider their possible dependence on the molar fraction of C_2F_6, and we write $k_1 = k_{10}\kappa_1(x_i)$ and $k_2 = k_{20}\kappa_2(x_i)$ in (6) and (7), with $\kappa_1(1) = \kappa_2(1) = 1$. If we then define ℓ_0 as the average

of the initial length of the bubbles, and:

$$\tau = \frac{\ell_0}{k_{10}}, \tag{8}$$

we can define dimensionless lengths $\bar{\ell}_i = \ell_i/\ell_0$ and time $\bar{t} = t/\tau$, and we get the dimensionless system:

$$\begin{cases} \mathrm{d}\bar{\ell}_i/\mathrm{d}\bar{t} = [\kappa_1(x_i) - \varepsilon\kappa_2(x_i)](-x_{i-1} + 2x_i - x_{i+1}) \\ \mathrm{d}x_i/\mathrm{d}\bar{t} = -[\kappa_1(x_i)x_i + \varepsilon\kappa_2(x_i)(1-x_i)](-x_{i-1} + 2x_i - x_{i+1})/\bar{\ell}_i \end{cases}, \tag{9}$$

where $\varepsilon = k_{20}/k_{10}$. The initial conditions at $\bar{t} = 0$ are: $x_i = 1$, and $\bar{\ell}_i = \ell_i(\bar{t} = 0)/\ell_0$. Combining the two equations of the dimensionless system, we thus get that the evolutions of $\bar{\ell}_i$ and x_i are correlated through the relation:

$$\frac{\bar{\ell}_i(\bar{t})}{\bar{\ell}_i(\bar{t}=0)} = \exp\left[\int_{x_i(\bar{t})}^{1} \frac{\kappa_1(x) - \varepsilon\kappa_2(x)}{\kappa_1(x)x + \varepsilon\kappa_2(x)(1-x)}\mathrm{d}x\right]. \tag{10}$$

If gas 2 is much less soluble than gas 1, a fairly good approximation for fluorinated gases compared to "simple" gases as N_2, we may neglect its solubility and we can solve approximately the previous model setting $\varepsilon = 0$. In this case, (10) reduces to $\bar{\ell}_i(\bar{t}) = \bar{\ell}_i(\bar{t} = 0)/x_i(\bar{t})$, hence (9) reduces to:

$$\frac{\mathrm{d}x_i}{\mathrm{d}\bar{t}} = -\frac{\kappa_1(x_i)x_i^2(-x_{i-1} + 2x_i - x_{i+1})}{\bar{\ell}_i(\bar{t}=0)}. \tag{11}$$

The system (9) is a general model on which we can compare our data. However, we will see in the upcoming Section that the continuous limit of this model at large number of bubbles provides a simpler and deeper understanding of the evolution process, in terms of effective diffusion.

Effective diffusion approach

If the number of bubbles is large, we can treat the variable i as continuous, and replace $x_i(t)$ by a function of two variables $x(i,t)$, and the term $-x_{i-1}+2x_i-x_{i+1}$ by $-\partial^2 x/\partial i^2$ in all above equations, which then resemble nonlinear diffusion equations. However, a difference is that the usual spatial variable appearing in diffusion equations is here replaced by a "topological distance", i; thus, the characteristic coefficient is not a diffusion coefficient, but the inverse time scale τ^{-1}. To get a diffusion coefficient which has the usual unit (and can be expressed in $\mathrm{m}^2{\cdot}\mathrm{s}^{-1}$), we must introduce the characteristic length ℓ_0 of the bubbles in the direction of diffusion. From the definition (8) of τ, we thus get the diffusion coefficient:

$$D = \frac{\ell_0^2}{\tau} = k_{10}\ell_0. \tag{12}$$

This coefficient is proportional to the typical size of the bubbles, because each gas/liquid interface to be crossed in the direction of the gas composition gradient acts as a barrier for the gas transfer. It is very useful, since it quantifies the efficiency of gas transfer through a foam.[29]

If we neglect the solubility of gas 2 compared to that of gas 1, the continuous model takes the form of a nonlinear diffusion equation, from (11):

$$\frac{\partial x}{\partial \bar{t}} = \frac{1}{\bar{\ell}(i,\bar{t}=0)}\kappa_1(x)x^2\frac{\partial^2 x}{\partial i^2}, \tag{13}$$

with initial condition $x(i,\bar{t}=0)=1$ and boundary conditions: $x(i=0,\bar{t})=0$ (because the first bubble is constantly in contact with pure N_2), and $\lim_{i\to\infty} x(i,\bar{t})=1$. The simplest case arises when all bubbles have initially the same length. Then $\bar{\ell}(i,\bar{t}=0)=1$, and (13) takes the form:

$$\frac{\partial x}{\partial \bar{t}} = \kappa_1(x)x^2\frac{\partial^2 x}{\partial i^2}, \tag{14}$$

which, together with the initial and boundary conditions, admits a self-similar solution of

the form: $x(i,t) = f(\xi)$, with $\xi = i/\bar{t}^{1/2}$. The function f obeys the ODE:

$$\kappa_1(f) f^2 f'' + \frac{1}{2}\xi f' = 0, \tag{15}$$

where primes indicate derivation with respect to ξ, and with boundary conditions :

$$f(0) = 0, \qquad \lim_{\xi \to +\infty} f(\xi) = 1. \tag{16}$$

The latter condition means that we consider an infinite foam. In experiments, although the number of bubbles is of course finite (at least equal to 30), no evolution was detectable for i larger than 13 (Fig. 2a), hence the experimental results do not depend on the deepest bubbles, which ensures that the approximation of an infinite foam is justified.

We shall test two possible models for κ_1; first, a constant permeability: $\kappa_1(f) = 1$, in which case (15) becomes $f^2 f'' + \frac{1}{2}\xi f' = 0$; second, an inverse law: $\kappa_1(f) = 1/f$ as suggested by the experiments of Hadji et al.,[24] in which case (15) becomes $f f'' + \frac{1}{2}\xi f' = 0$. These two problems are solved numerically, and the corresponding solutions for $f(\xi)$ and $f'(\xi)$ are plotted in Fig. 3 and its inset, respectively.

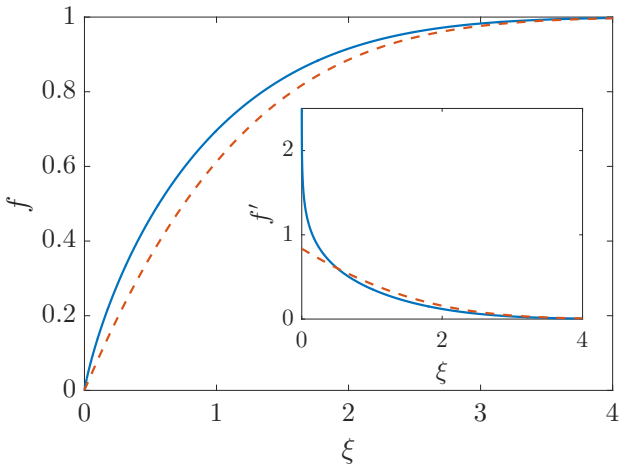

Figure 3: Plot of the numerical solution $f(\xi)$ of Eq. (15) with boundary conditions (16) for $\kappa_1(f) = 1$ (plain line) and $\kappa_1(f) = 1/f$ (dashed line). Inset: plot of $f'(\xi)$.

This theoretical analysis suggests that the experimental time evolution of the various

bubbles can be rescaled, if the system is initially monodisperse. To test this idea, we replot in Fig. 4 the data from Fig. 2, initially prepared as monodisperse as possible, as a function of ξ. Technically, to have a better assessment of rescaling, we plot $\ell/\ell(t=0)-1$ as a function of ξ, in log-log representation. This shows that indeed, all data collapse very well on single curves. The deviations from the rescaling are seen for the bubble closest to the free end, which is expected since replacing the term $-x_{i-1}+2x_i-x_{i+1}$ by a Laplacian is formally allowed only if x_{i-1}, x_i and x_{i+1} have little relative variations, which of course does not hold true close to the free end where variations of molar fraction are sharp. Another deviation is seen in Fig. 4c, this time for bubbles deeper down in the foam. In this case, a possible reason for the lack of rescaling is the variation between the initial lengths of the bubbles, which breaks the self-similarity. Indeed, that particular experiment is the less initially monodisperse amongst the three reported experiments (see insets of Fig. 2).

To test further the applicability of the self-similar approach, we fit the rescaled data by the solution of (15) with boundary conditions (16). Since Fig. 4 displays $\ell/\ell(t=0)-1$ as a function of $i/t^{1/2}$, the corresponding data must be compared to $f(\xi/\tau_{\rm fit}^{1/2})^{-1}-1$, with $\tau_{\rm fit}$ a characteristic time. For the comparison between the data and the model, we use $\tau_{\rm fit}$ as a single fitting parameter for all data. Fig. 4 shows that the agreement between the rescaled data and the model is very good. We can extract from the value of $\tau_{\rm fit}$ a measurement of the permeability k_{10} using (8). We recall that this parameter is simply the permeability of N_2 in the constant-permeability model, and the permeability of N_2 at $x=1$ in the variable-permeability model. We obtain a value of the permeability equal to $k_{10}=3.0\times10^{-5}$ m/s in the constant-permeability model, and $k_{10}=2.3\times10^{-5}$ m/s in the variable-permeability model. The two models give very similar curves on Fig. 4, hence it is difficult to discriminate between them from this data representation. Overall, the good agreement between the data and the continuous model fully validates the effective diffusion approach to understand the transfer of N_2 through the foam.

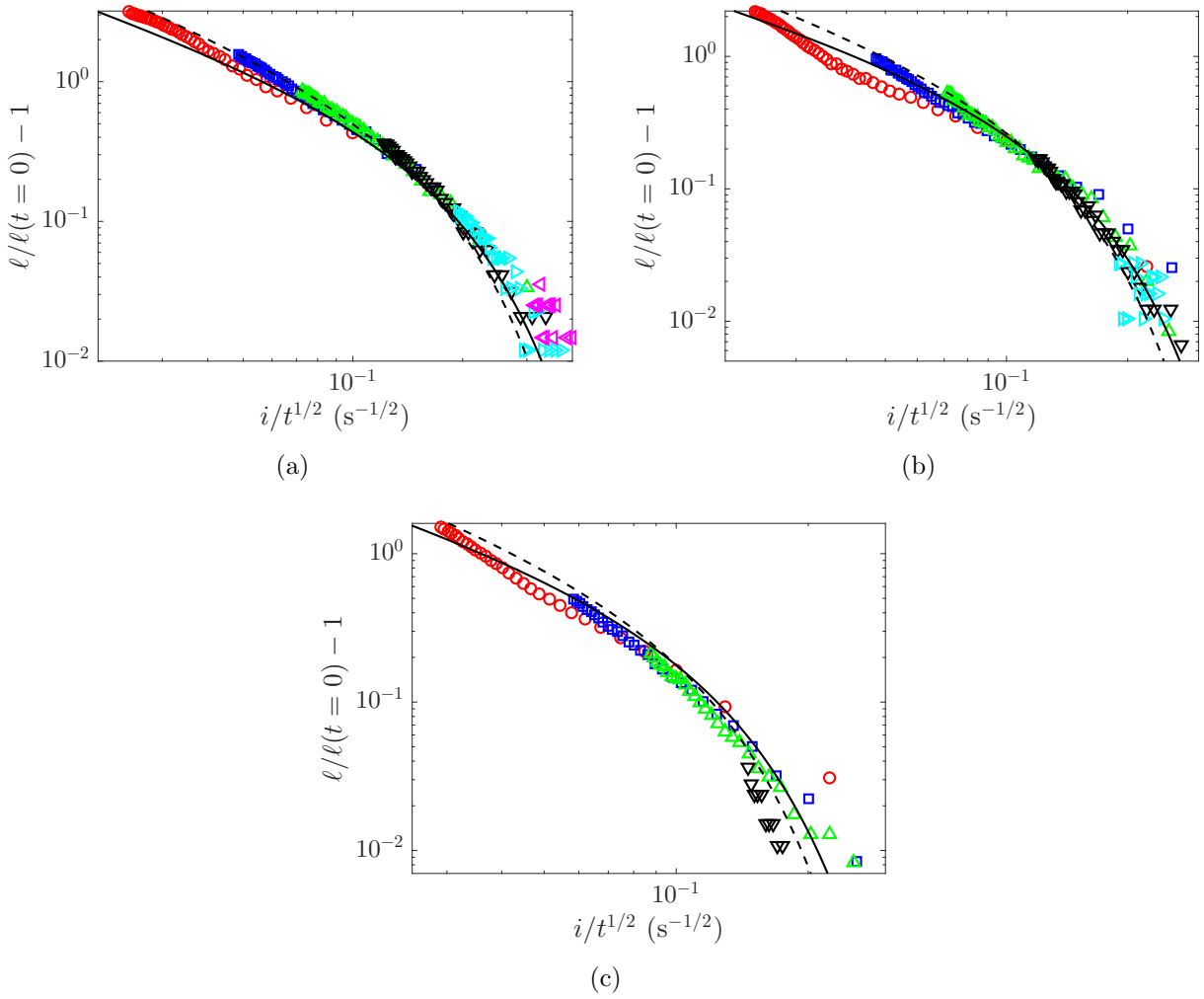

Figure 4: Same data as in Fig. 2: (a) data from Fig. 2a, (b) data from Fig. 2b, (c) data from Fig. 2c, but plotted as a function of the self-similar variable $\xi = i/t^{1/2}$. The curves are best fit of the solution of (15) with boundary conditions (16), for $\kappa_1(f) = 1$ in plain line (constant-permeability model), and $\kappa_1(f) = 1/f$ in dashed line (variable-permeability model).

Discussion of the permeability

The value of the permeabilities is essential to use the model, and we now discuss them. The general formula for the permeability for a given gas through a soap film is:[18]

$$\frac{1}{k} = \frac{h}{D\mathrm{He}} + \frac{2}{k_{\mathrm{ML}}}, \tag{17}$$

where the first term in the r.h.s. comes from the transport in the bulk, and the second one from the transport across the two adsorbed monolayers at the gas/liquid interfaces bounding the film, whence the subscript ML standing for "monolayer" in the last term of (17). In the first term, D is the gas diffusivity in water, He Henry's constant (defined here as the dimensionless ratio of the aqueous-phase concentration of a species and its gas-phase concentration) and h the average film thickness. Experimental tables give $D_1 = 2.0 \times 10^{-9}$ m^2/s, $\mathrm{He}_1 = 0.016$ (^{2}) for N_2, and $D_2 = 8.6 \times 10^{-6}$ m^2/s, $\mathrm{He}_2 = 1.4 \times 10^{-3}$ for C_2F_6; see[30] and references therein for these values for C_2F_6. From these values, we compute $D_2\mathrm{He}_2/D_1\mathrm{He}_1 = 0.037$, which shows that the resistance to transfer through the liquid is much larger for C_2F_6 than for N_2.

Tcholakova et al.[4] measured the following air permeability with the surfactant mixture which we use: $(8 \pm 2) \times 10^{-5}$ m/s from the analysis of a coarsening foam, and $(11 \pm 3) \times 10^{-5}$ m/s from the diminishing bubble method. This order of magnitude of 10^{-4} m/s is one order of magnitude lower than the permeability reported with "simple" surfactant solutions. For instance, Princen & Mason[18] measured an air permeability of 1.4×10^{-3} m/s with a hexadecyltrimethylammonium bromide (HTAB) solution. Tcholakova et al.[4] ascribed this large reduction in permeability to the efficiency of the adsorption layers formed by the myristic acid at the gas/liquid interfaces as a barrier for the gas transfer. In such systems, this barrier effect largely dominate the resistance to transfer due to the bulk of liquid within the foam, which we shall henceforth neglect. In the rest of the discussion, we will identify these air permeabilities with that of N_2, which is largely correct when discussing orders of

magnitude. For instance, Princen & Mason[18] measured N_2 permeability of 1.2×10^{-3} m/s in their system, which is only 15% lower than that of air.

However, we have estimated in the previous Section a permeability of order 3×10^{-5} m/s, which is even lower than the permeability measured by Tcholakova et al.[4] This suggests that yet another mechanism of resistance to transfer is at play when C_2F_6 is used. It echoes the experiments by Hadji et al.,[24] who studied air transfer through a single soap film from a bubble containing pure air to a bubble containing a mixture of air and of insoluble C_6F_{14} vapour. They showed that the permeability was decreasing at increasing molar fraction of C_6F_{14}, an effect which they ascribed to the adsorption of C_6F_{14} molecules at gas/liquid interfaces. Such an adsorption of fluorinated gases was also reported in other studies, and was shown to modify various interfacial properties, notably surface tension.[31–33] More precisely, Hadji et al. showed that the permeability was varying, as a good approximation, as the inverse of the molar fraction of C_6F_{14}.

To test this result, a way to quantify the permeability consists in using Eq. (4) from the model to directly estimate k_1: by measuring the variation rate of length $\mathrm{d}\ell_i/\mathrm{d}t$ and the quantity $-x_{i-1} + 2x_i - x_{i+1}$, we can infer the permeability from the experimental data. The quantity $\mathrm{d}\ell_i/\mathrm{d}t$ is straightforward to extract from the data by finite differences. However, even though we smoothed the data over five data points prior to estimate $\mathrm{d}\ell_i/\mathrm{d}t$, it remains extremely noisy, except for the first bubble, on which we shall henceforth restrict the analysis. Moreover, assuming C_2F_6 is insoluble, its molar fraction x_i in bubble i is directly related to the current length ℓ_i and the initial length ℓ_{i0}: $x_i = \ell_{i0}/\ell_i$. Hence for bubble 1, knowing that the exterior is saturated by N_2, one has:

$$(-x_{i-1} + 2x_i - x_{i+1})|_{i=1} = -1 + 2\frac{\ell_{10}}{\ell_1} - \frac{\ell_{20}}{\ell_2}, \tag{18}$$

and from (4), the permeability is estimated as:

$$k_1 = \left(-1 + 2\frac{\ell_{10}}{\ell_1} - \frac{\ell_{20}}{\ell_2}\right)^{-1} \frac{\mathrm{d}\ell_i}{\mathrm{d}t}. \tag{19}$$

We plot the permeability as a function of the molar fraction of C_2F_6 in Fig. 5. Despite significant scattering, this figure indeed suggests that the permeability is a decreasing function of the molar fraction of C_2F_6. A fit with an inverse law is in reasonable agreement with the data, although the variation of the experiments is sharper than that of an inverse law in a range of molar fraction between 0.4 and 0.6, while the data increase in a narrow range between 0.25 and 0.30 for one experiment. It is difficult to be more conclusive, given the limited range of accessible molar fractions, itself due to the limited stability of the films. Moreover, the films themselves have a strong internal dynamics (e.g. due to marginal regeneration)[34,35] which may transport the adsorbed species, and make their permeability fluctuate over time. Finally, the fitting parameter extracted from Fig. 5, $k_{10} = 1.0 \times 10^{-5}$ m/s, is significantly lower than the one extracted from the effective diffusion approach and reported in the previous section, $k_{10} = 2.3 \times 10^{-5}$ m/s. Although we have no clear reason to explain this discrepancy, the film in contact with the exterior experiences forced convection currents owing to the continuous supply of N_2, which may strongly perturb the permeability as compared to all other films which do not experience convection.

Finally, we must discuss some simplifying assumptions made in deriving the model. First, we assume a thin film spanning all the tube, neglecting the presence of the Plateau borders which are known to hinder or block gas transfer in other coarsening studies,[36] because of the prohibitive bulk distance to cross for the molecules of the dissolved gas. It is difficult to estimate the radius of the Plateau borders in our images, due to the optical distortions associated with the cylindrical tube geometry. As a rough estimate, they occupy typically 10% of the tube radius (Fig. 1b). Therefore, our permeabilities are underestimated by about 10%. Second, we have assumed that the gases are instantaneously mixed within each

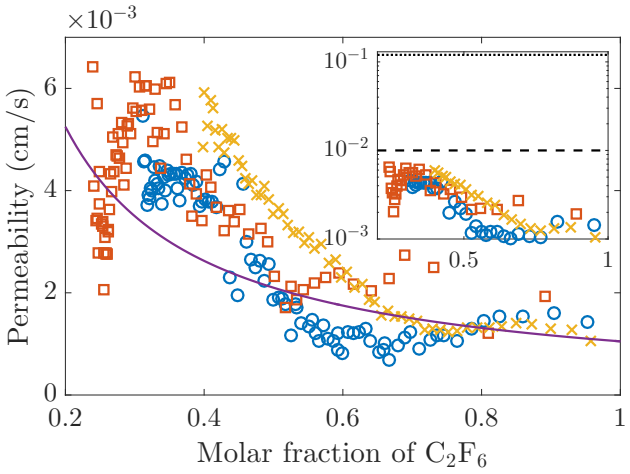

Figure 5: Plot of the permeability as a function of the molar fraction x_1 of C_2F_6 for the first bubbles of the three experiments from Fig. 2a ($\circ$), b ($\square$) and c ($\times$), and fit of the data by a trend $k_1 = k_{10}/x_1$, with best fitting parameter $k_{10} = 1.0 \times 10^{-5}$ m/s. Inset: semi-log plot of the same data, together with the values from Princen & Mason[18] (dotted line) and from Tcholakova et al.[4] (dashed line).

bubble. This holds true because the mutual diffusivity of N_2 and C_2F_6 in gas phase, equal to 7×10^{-6} m^2/s, is much larger than the effective diffusivity (12): $D = k_1\ell$, of order 10^{-7} m^2/s in our study.

Conclusions

In this study, we have reported on the evolution of a bamboo foam made of a relatively insoluble gas (C_2F_6) and placed in contact with a reservoir of a soluble gas (N_2). We have shown that the foam swells, as the bubble continuously incorporate the soluble gas, the bubbles being at closer distance from the reservoir growing sooner and faster. We have rationalised our observations by a model based on a linear law between the gas fluxes and the difference in molar fractions (or concentrations) across films. In the limit of a large number of bubbles, the model tends to an effective nonlinear diffusion process, the nonlinearity stemming from the dilution of the insoluble by the soluble one. Such a continuous approach reproduces the experimental dynamics very well. The order of magnitude of the diffusion coefficients is given by the product of the permeability of the soluble gas and the initial

bubble size. This effective diffusion approach is important for application, since it enables to estimate the dynamics of gas exchange in a bulk of foam.

Interestingly, this effective diffusion constant echoes the one introduced in Ostwald ripening of foams,[30] but with an important difference: in our case, gas exchanges are driven by gradients of partial pressure, which scale as P_{atm}, while in Ostwald ripening, they are driven by gradients of Laplace pressure, which scale as the ratio of the surface tension by the bubble size, which is typically two or three orders of magnitude lower than the atmospheric pressure. Consequently, the effective diffusion introduced in our study is much larger than the one appearing in Ostwald ripening, hence the gas transfers are much faster.

On a more specific standpoint, our results also confirm the "blocking" effect of fluorinated gases, probably because they form adsorption layers at interface acting as barriers. However, our results also tend to show that the efficiency of this barrier decreases as the fluorinated gas is diluted by the permeation of a more soluble gas. More studies would be helpful to characterise these interfacial adsorption layers as a function of the partial pressure, or to predict the permeability from the molecular properties of the gases and surfactants involved at the interfaces.

Acknowledgement

The author thanks Élise Lorenceau for many fruitful discussions about gas transfer through foams.

References

(1) Cantat, I.; Cohen-Addad, S.; Elias, F.; Graner, F.; Höhler, R.; Pitois, O.; Rouyer, F.; Saint-Jalmes, A. In *Foams, Structure and Dynamics*; Cox, S. J., Ed.; Oxford University Press: Oxford, 2013.

(2) Sander, R. Compilation of Henry's law constant (version 4.0) for water as solvent. *Atmos. Chem. Phys.* **2015**, *15*, 4399–4981.

(3) Blijdenstein, T. B. J.; de Groot, P. W. N.; Stoyanov, S. D. On the link between foam coarsening and surface rheology: why hydrophobins are so different. *Soft Matter* **2010**, *6*, 1799–1808.

(4) Tcholakova, S.; Mitrinova, Z.; Golemanov, K.; Denkov, N. D.; Vethamuthu, M.; Ananthapadmanabhan, K. P. Control of Ostwald ripening by using surfactants with high surface modulus. *Langmuir* **2011**, *27*, 14807–14819.

(5) Tcholakova, S.; Mustan, F.; Pagureva, N.; Golemanov, K.; Denkov, N. D.; Pelan, E. G.; Stoyanov, S. D. Role of surface properties for the kinetics of bubble Ostwald ripening in saponin-stabilized foams. *Colloids Surf. A* **2017**, *534*, 16–25.

(6) Briceño-Ahumada, Z.; Langevin, D. On the influence of surfactant on the coarsening of aqueous foams. *Adv. Colloid Interface Sci.* **2017**, *244*, 124–131.

(7) Martínez, A. C.; Rio, E.; Delon, G.; Saint-Jalmes, A.; Langevin, D.; Binks, B. P. On the origin of the remarkable stability of aqueous foams stabilised by nanoparticles: link with microscopic surface properties. *Soft Matter* **2008**, *4*, 1531–1535.

(8) Rio, E.; Drenckhan, W.; Salonen, A.; Langevin, D. Unusually stable liquid foams. *Adv. Colloid Interface Sci.* **2014**, *205*, 74–86.

(9) Webster, A. J.; Cates, M. E. Stabilization of emulsions by trapped species. *Langmuir* **1998**, *14*, 2068–2077.

(10) Webster, A. J.; Cates, M. E. Osmotic stabilization of concentrated emulsions and foams. *Langmuir* **2001**, *17*, 595–608.

(11) Saint-Jalmes, A. Physical chemistry in foam drainage and coarsening. *Soft Matter* **2006**, *2*, 836–849.

(12) Gandolfo, F. G.; Rosano, H. L. Interbubble gas diffusion and the stability of foams. *J. Colloid Interface Sci.* **1997**, *194*, 31–36.

(13) Steck, K.; Hamann, M.; Andrieux, S.; Muller, P.; Kékicheff, P.; Stubenrauch, C.; Drenckhan, W. Fluorocarbon vapors slow down coalescence in foams. *Adv. Mater. Interfaces* **2021**, *8*, 2100723.

(14) Maurdev, G.; Saint-Jalmes, A.; Langevin, D. Bubble motion measurements during foam drainage and coarsening. *J. Colloid Interface Sci.* **2006**, *300*, 735–743.

(15) Pierre, J.; Dollet, B.; Leroy, V. Resonant acoustic propagation and negative density in liquid foams. *Phys. Rev. Lett.* **2014**, *112*, 148307.

(16) Elias, F.; Crassous, J.; Derec, C.; Dollet, B.; Drenckhan, W.; Gay, C.; Leroy, V.; Noûs, C.; Pierre, J.; Saint-Jalmes, A. The acoustics of liquid foams. *Curr. Opin. Colloid Interface Sci.* **2020**, *50*, 101391.

(17) Pierre, J.; Giraudet, B.; Chasle, P.; Dollet, B.; Saint-Jalmes, A. Sound propagation in liquid foams: Unraveling the balance between physical and chemical parameters. *Phys. Rev. E* **2015**, *91*, 042311.

(18) Princen, H. M.; Mason, S. G. Permeability of soap films to gases. *J. Colloid Interface Sci.* **1965**, *20*, 353–375.

(19) Nedyalkov, M.; Krustev, R.; Kashchiev, D.; Platikanov, D.; Exerowa, D. Permeability of Newtonian black foam films to gas. *Colloid Polymer Sci.* **1988**, *266*, 291–296.

(20) Ramanathan, M.; Müller, H. J.; Möhwald, H.; Krastev, R. Foam films as thin liquid gas separation membranes. *ACS Appl. Mater. Interfaces* **2011**, *3*, 633–637.

(21) Reznickova, J.; Petrychkovych, R.; Vejrazka, J.; Setnickova, K.; Uchytil, P. Gas separation ability of the liquid bubble film. *Sep. Purif. Technol.* **2016**, *166*, 26–33.

(22) Cook, R. L.; Tock, R. W. Aqueous membranes for the separation of gaseous mixtures. *Sep. Sci.* **1974**, *9*, 185–193.

(23) Farajzadeh, R.; Krastev, R.; Zitha, P. L. J. Foam film permeability: Theory and experiment. *Adv. Colloid Interface Sci.* **2008**, *137*, 27–44.

(24) Hadji, C.; Dollet, B.; Bodiguel, H.; Drenckhan, W.; Coasne, B.; Lorenceau, E. Influence of fluorocarbon gaseous environment on the permeability of foam films to air. *Langmuir* **2020**, *36*, 13236–13243.

(25) Sujatha, K.; Das, T. R.; Kumar, R.; Gandhi, K. S. Permeation of gases through liquid films. *Chem. Eng. Sci.* **1988**, *43*, 1261–1268.

(26) Weaire, D.; Pageron, V. Frustrated froth: evolution of foam inhibited by an insoluble gaseous component. *Phil. Mag. Lett.* **1990**, *62*, 417–421.

(27) Quoc, P. N.; Zitha, P. L. J.; Currie, P. K. Effect of foam films on gas diffusion. *J. Colloid Interface Sci.* **2002**, *248*, 467–476.

(28) Golemanov, K.; Denkov, N. D.; Tcholakova, S.; Vethamuthu, M.; Lips, A. Surfactant mixtures for control of bubble surface mobility in foam studies. *Langmuir* **2008**, *24*, 9956–9961.

(29) Trinh, P.; Mikhailovskaya, A.; Lefèvre, G.; Pantoustier, N.; Perrin, P.; Lorenceau, E.; Dollet, B.; Monteux, C. Relation between oxidation kinetics and reactant transport in an aqueous foam. *J. Colloid Interface Sci.* **2023**, *643*, 267–275.

(30) Hilgenfeldt, S.; Koehler, S. A.; Stone, H. A. Dynamics of coarsening foams: Accelerated and self-limiting drainage. *Phys. Rev. Lett.* **2001**, *86*, 4704–4707.

(31) Mucic, N.; Moradi, N.; Javadi, A.; Aksenenko, E. V.; Fainerman, V. B.; Miller, R. Mixed adsorption layers at the aqueous C(n)TAB solution/hexane vapour interface. *Colloids Surf. A* **2014**, *442*, 50–55.

(32) Krafft, M. P.; Fainerman, V. B.; Miller, R. Modeling of the effect of fluorocarbon gases on the properties of phospholipid monolayers and the adsorption dynamics of their aqueous solutions or dispersions. *Colloid Polymer Sci.* **2015**, *293*, 3091–3097.

(33) Shi, D.; Counil, C.; Krafft, M. P. Fluorocarbon exposure mode markedly affects phospholipid monolayer behavior at the gas/liquid interface: Impact on size and stability of microbubbles. *Langmuir* **2019**, *32*, 12461–12467.

(34) Mysels, K. J.; Shinoda, K.; Frenkel, S. *Soap Films, Studies of Their Thinning and a Bibliography*; Pergamon Press: New York, 1959.

(35) Gros, A.; Bussonnière, A.; Nath, S.; Cantat, I. Marginal regeneration in a horizontal film: Instability growth law in the nonlinear regime. *Phys. Rev. Fluids* **2021**, *6*, 024004.

(36) Schimming, C. D.; Durian, D. J. Border-crossing model for the diffusive coarsening of two-dimensional and quasi-two-dimensional wet foams. *Phys. Rev. E* **2017**, *96*, 032805.

TOC Graphic

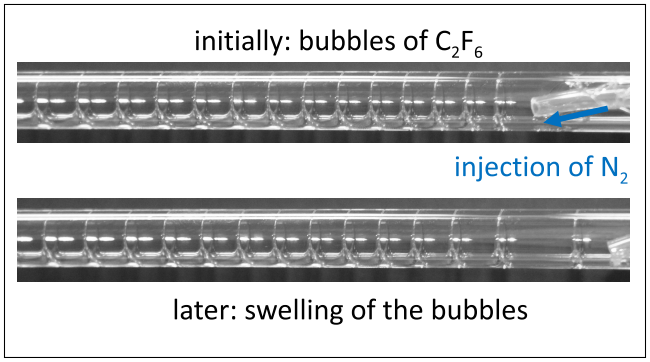
initially: bubbles of C_2F_6
injection of N_2
later: swelling of the bubbles

TOC Graphic

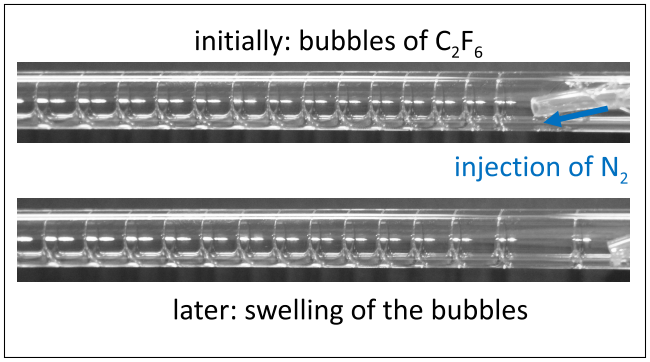
initially: bubbles of C_2F_6
injection of N_2
later: swelling of the bubbles